Eur. Phys. J. B **59**, 329–342 (2007)
DOI: 10.1140/epjb/e2007-00300-7

THE EUROPEAN PHYSICAL JOURNAL B

Multi-photon behaviors of shot noise in a quantum dot system under the perturbation of two microwave fields

Hong-Kang Zhao[1,2,a] and Jian Wang[2]

[1] Department of Physics, Beijing Institute of Technology, Beijing 100081, P.R. China
[2] Department of Physics and the Center of Theoretical and Computational Physics, The University of Hong Kong, Pokfulam Road, Hong Kong, P.R. China

Received 27 June 2007 / Received in final form 3 August 2007
Published online 1st November 2007

Abstract. We have investigated the shot noise affected by the perturbation of two microwave fields (MWFs) with frequencies ω_1 and ω_2, which can be classified as the commensurate and incommensurate external ac fields. The time-dependent current correlation function and the spectral density of shot noise have been obtained. They are very different compared with the single-field applied system in the nonlinear regime of the ac potentials. The different photon absorption and emission processes induce different kinds of noise spectral density. We have performed the numerical calculations for both commensurate balanced and unbalanced photon absorptions and emissions. The multi-photon procedure can be seen clearly from the resonance of shot noise. Different commensurate number $q = \omega_2/\omega_1$ contributes to different photon absorption and emission behaviors. It is found that the asymmetric configuration of shot noise is intimately associated with the commensurate number q. The differential conductance appears symmetric and asymmetric behaviors, and the channel blockade exhibits. The shot noise is large enough to surpass its saturated value for the unbalanced photon absorption case. The sensitive behaviors of Fano factor associated with different commensurate numbers and amplitudes of ac fields signify that the shot noise can be controlled by external MWFs significantly.

PACS. 72.10.Bg General formulation of transport theory – 73.21.La Quantum dots – 73.23.-b Electronic transport in mesoscopic systems – 85.35.-p Nanoelectronic devices

1 Introduction

The development of nanotechnology stimulates the investigation of ultra-small devices theoretically and experimentally. On one hand, to explore the new physics we develop necessary theoretical techniques and approaches. On the other hand, the theoretically revealed physical features on the nanostructure are used for designing new electronic devices. The phase coherence plays crucial role in electronic transport through such small systems because the dimensions of these devices are smaller than or comparable with the phase coherence lengths. Due to the interferences of electron wave packets, the quantum effects appear clearly at low temperature. For new devices in the electronic circuit and equipment, it is important to study their characteristics in order to control the output signals through changing the external parameters.

From the practical point of view, the devices are usually operated in the presence of radio frequency electromagnetic fields or microwave fields (MWFs) for controlling the tunneling behaviors of the charge carriers [1,2]. The ac perturbations can give rise to very interesting phenomena, such as photon-electron pumping effect related to Rabi oscillation between the states of double quantum dot (QD) mesoscopic system [3]. For this reason the study of the influences of ac fields on the transport properties in nanostructures has become an increasingly interesting subject [4–12]. The pioneer work on the photon-assisted tunneling was performed by Tien and Gordon in 1960s for studying the photon absorption and emission effect in superconducting tunneling devices [13]. The perturbation of MWF induces side-band $E + n\hbar\omega$ to modify the energy level E, and the tunneling electrons may absorb ($n > 0$) and emit ($n < 0$) photons. The observation of photon-assisted tunneling was achieved by Kouwenhoven et al. to find transport features with a linear frequency dependence in a QD system [1]. The electrons can overcome the Coulomb gap in the QD when the discrete photon energies are absorbed from the applied microwaves [14]. Although the theoretical model is chosen as a single-level

[a] e-mail: zhaohonk@yahoo.com

QD without considering the Coulomb interaction [7], the shape and structure of the photon-assisted tunneling are in good agreement with the experiment stated in reference [1]. The photon-electron quantum pumps have been investigated intensively during the past decades due to applying alternating voltages to produce nonzero direct current [15–19]. The various methods are employed for treating the time-dependent transport, such as time-dependent Schrödinger equation relating to the Floquet theory [11], the master equation [4,20,21], the nonequilibrium Green's function (NGF) technique [5–8,22,23], the random matrix theory [24], and the scattering matrix [8,25].

In mesoscopic systems, high-frequency and strong ac fields usually may produce nontrivial quantum effects, which should be treated by nonadiabatic approach. The nonlinear behaviors are expected to display novel physics and structures associated with tunneling current and frequency-dependent conductance. In studying time-dependent mesoscopic systems, the NGF approach provides us a very convenient way to deal with the nonlinear transport. It also allows us to solve the problems self-consistently beyond elastic scattering. This method is suitable for the systems associated with the experimentally measurable nonadiabatic mesoscopic transport as the frequencies of the applied fields reach tens of THz [22].

The shot noise is a nonequilibrium fluctuation which is caused by the discreteness of the charge carriers [25,26]. The momentum noise of barriers in the single-channel approximation by using a second quantization [27], the quasi-classical discussion of fluctuation with a view of ballistic transport [28] have been investigated. When the size of an electronic system reaches the nanometer scale, noise becomes a very interesting problem. As the sample gets smaller, its charging energy increases and eventually becomes larger than the thermal energy. Electrons traveling through a device become correlated in the same channel and same probe, as well as in different channels and different probes. In a macroscopic system, the generalized Nyquist current noise spectral density is related to the conductance. But in a mesoscopic system, this relation is valid only in very special conditions. Büttiker et al. used a scattering theory to study the dynamic conductance and shot noise at low-frequency, and obtained interesting results on these quantities [8,9,25]. Given the fact that the mesoscopic ac conductance has been extensively studied, the shot noise induced by the ac fields needs further investigation. During past years, the frequency dependence of noise spectrum has been studied by several authors [21,29–33] through different approaches for different systems. The excess noise in a quantum conductance in the presence of constant and alternating external fields has been studied to exhibit the singular dependence on the dc voltage and ac frequency [34]. The investigation on the deviations from the purely Poissonian shot noise in mesoscopic systems has been an increasingly interesting subject. For Poissonian distribution in a macroscopic system the current shows the value of shot noise by the well-known Schottky formula $S_P = 2e\langle I\rangle$. However, for a mesoscopic system, the electrons are correlated due to coherent transport, and they are governed by the Fermi distribution and Pauli principle. This quantum behavior results in the deviation of shot noise to the Poissonian distribution. The suppression [35–37] and enhancement [38–40] of shot noise have been discussed with different physical origin. Negative correlations between current pulses can lead to a complete suppression of the shot noise in quantum point contacts. From the investigation of noise in mesoscopic systems we can obtain additional information due to the interference of tunneling currents which is absence in the conductance. The transporting electrons in the perturbation of ac fields are highly correlated in time, the incident and outgoing electrons interfere with each other to induce very interesting physical phenomena. This also allows us for a better understanding electron transport in mesoscopic devices from the converse version.

This paper investigates the shot noise in a mesoscopic system under the perturbation of external ac fields, due to the microwave fields irradiating to the central QD. We are interested in the ac interference of current correlations induced by the two perturbations. We first derive the tunneling current operator, and then we derive the time-dependent current-current correlation. The noise spectral density is obtained by taking Fourier transformation. The novel features arise from the interference between different branches of currents, this in turn affects the shot noise of the system perturbed by the double MWFs. The information of MWFs is transferred to the tunneling currents, and therefore to the current noise. The selection rule is found from considering the energy conservation associated with photon absorption and emission procedures during electrons transport through the system. It is found that several procedures may exist in the double MWFs irradiated system, which is related to the commensurate (the two frequencies are commensurable) and incommensurate (the two frequencies are incommensurable) fields. In the literatures, one can find the two-signal perturbation systems associated with the investigation of tunneling current in the quantum pump [18,19], and photon-assisted current interference effect [41]. The frequencies of the perturbed fields can be divided into the commensurate and incommensurate cases, and the perturbations of different fields result in considerable different features of tunneling current and conductance. The main reason of the particular behaviors is arisen from the branch interference of electrons due to absorbing photon energies. This situation is most important for the nonlinear photon-assisted electron transport due to multi-photon absorption and emission procedure. One can imagine the case that electrons transporting through a mesoscopic system keep their phase coherence in the absence of external ac field. However, this coherence is broken down temporally due to absorbing and emitting photons when a single ac field is applied. On time average, the absorbed and emitted photons from the field satisfies energy conservation, and therefore we obtain the coherent electron transport to produce nonzero stair-like photon-assisted dc current. On the other hand, if we apply two commensurate fields, i.e., the frequency ratio number $\omega_2/\omega_1 = q$ is an integer, the phase coherence is

broken down temporally and more heavily due to absorbing and emitting of photons from the different fields. On time average, we also obtain the coherent electron tunneling since the electrons absorbing and emitting photons from the two fields keep energy conservation. This means that the absorbed photons from one field may be emitted to the other field, and the total number of the absorbed and emitted photons keeps unchanged by taking time-average. As a result, the compound effect of the tunneling current induced by the commensurate fields causes nontrivial transport behavior, and the novel features may exhibit through current and conductance, as well as the spectral density of noise. From the energy structure of the system, we find that some of the side-channels may overlap for the commensurate case, while we can not find the overlapping of side-channels for the incommensurate case. The main new results of this paper are listed in the following three aspects. (1) The asymmetric configuration of shot noise is intimately associated with the frequency ratio number (commensurate number)q. The shot noise is large enough to surpass its saturated value for the unbalanced photon absorption case. (2) For the case with $q = 1$, the differential conductance appears symmetric behavior, and the channel blockade exhibits due to the multi-photon absorption procedure. However for the case where $q > 1$, the peak suppression and enhancement induce asymmetric nonlinear differential conductance. (3) The sensitive behaviors of Fano factor associated with different commensurate number q and amplitudes of ac fields signify that the shot noise can be controlled by external MWFs significantly.

The paper is organized as the follows. The theoretical formalism is laid down in Section 2 where the time-dependent current-current correlation, and the shot noise spectral density are derived. The obtained formulas as the current operators, time-averaged current formula, and the spectral density of noise can be found in this section. Here we are interested in dealing with the double-signal perturbed system in the regime of nonlinear and nonadiabatic multi-photon procedure. Section 3 shows the numerical calculations of shot noise and Fano factor for the commensurate MWFs perturbation. The double-field perturbation results in novel features through numerical calculations, such as the photon blockade effect. The last section contributes to the concluding remarks.

2 Hamiltonian and formalism

The system we considered is composed of three subsystems: the double-barrier QD, the left and right leads connected to two equilibrium electron reservoirs. The two leads are biased by a dc voltage V. The difference of chemical potentials μ_L and μ_R relates the voltage by $eV = \mu_L - \mu_R$, where the voltage is not necessarily small. The QD is irradiated with two MWFs through the gate of QD. The application of MWFs can be expressed by the potentials $eV_j \cos(\omega_j t)$ $(j = 1, 2)$ if the fields are introduced periodically in the dipole approximation. The tunneling electrons carry the information of the external MWFs, and the interference of currents induces nontrivial behaviors associated with the nature of MWFs. We assume that the fields are finite for V_j and ω_j in general, and nonlinear effect may exist in the system as the voltages are large. The frequencies of the fields can reach THz associated with nonadiabatic phenomena [22]. Experimentally, such high frequency applied photon-assisted tunneling has been observed by Guimarães et al. through choosing the free-electron lasers as the source of terahertz electric fields [42]. Generally, the Coulomb interaction U exists in the electron system, and the interaction becomes stronger as the sample becomes smaller. However, we can restrict our investigation to consider the tunneling in the neighborhood of a single Coulomb oscillation peak [31,43,44]. The theoretical consideration on this restriction can be described by a single channel QD model approximately as long as the measurement of the voltages and photon energies are much smaller than the level space and Coulomb interaction U, i.e., $\hbar\omega_i \ll \Delta E_1 < U$, where ΔE_1 is the energy space between the first and second energy levels of QD. The experimental observation for the physics around this level can be achieved by detecting the tunneling behaviors and noise near this energy region.

In order to grasp the essential feature of the double-field induced nonlinear multi-photon behaviors, we employ the simple model without Coulomb interaction. The Hamiltonian of the QD system with two MWFs applying to the QD can be written as

$$H = \sum_{\gamma\in\{L,R\}} \sum_{k\sigma} E_{\gamma,k} a^{\dagger}_{\gamma,k\sigma} a_{\gamma,k\sigma} + \sum_{\sigma} \varepsilon_d(t) d^{\dagger}_{\sigma} d_{\sigma} + \sum_{\gamma\in\{L,R\}} \sum_{k\sigma} \Big(R_{\gamma k} a^{\dagger}_{\gamma,k\sigma} d_{\sigma} + \text{H.C.} \Big), \quad (1)$$

where $\varepsilon_d(t) = E_d + \sum_{i=1}^{2} eV_i \cos(\omega_i t)$, and E_d is the energy level of an electron in the QD for our spin degenerate system. V_i and ω_i represent the magnitude and angular frequency of the ith field. $E_{\gamma,k}$ represents the energy level of an electron in the γth lead. $a^{\dagger}_{\gamma,k\sigma}$, and $a_{\gamma,k\sigma}$ denote the creation and annihilation operators of electron in the leads. $d^{\dagger}_{\sigma}$, and d_{σ} are the creation and annihilation operators of electron in the QD. The electrons in the QD are coupled to the electrons in the leads by tunneling strengths $R_{\gamma k}$. This model describes the situation that two microwave signals are applied simultaneously to the quantum device through gate. The tunneling current is affected by the two fields, and the modulation of MWFs gives rise to perturbation terms in QD. In order to proceed the derivation conveniently, we make a gauge transformation over the Hamiltonian. This gauge transformation can be achieved by taking the transformation over the wavefunction of the system as $\Psi(t) = \hat{U}(t)\widetilde{\Psi}(t)$, where the unitary operator is determined by $\hat{U}(t) = \exp[-i \sum_{\sigma} \sum_{j=1}^{2} \lambda_j d^{\dagger}_{\sigma} d_{\sigma} \sin(\omega_j t)]$. We have defined the scaled magnitudes of the MWFs by $\lambda_j = eV_j/\hbar\omega_j$. Due to this transformation, the time-dependent term is canceled from the energy $\varepsilon_d(t)$. However, the Schrödinger

equation changes to $i\hbar\partial\widetilde{\Psi}(t)/\partial t = \widetilde{H}\widetilde{\Psi}(t)$, where $\widetilde{H} = \hat{U}(t)^{-1}H'\hat{U}(t)$, and H' is the Hamiltonian associated with equation (1), but without the time-oscillation energy. To obtain the explicit form of the Hamiltonian $\widetilde{H}$, we note the relations $d_\sigma\hat{U}(t) = \exp[-i\sum_{j=1}^{2}\lambda_j\sin(\omega_j t)]\hat{U}(t)d_\sigma$, $d_\sigma^\dagger\hat{U}(t) = \exp[i\sum_{j=1}^{2}\lambda_j\sin(\omega_j t)]\hat{U}(t)d_\sigma^\dagger$, and the commutation relation $[a_{\gamma,k\sigma}, \hat{U}(t)] = 0$. We therefore obtain the Hamiltonian $\widetilde{H}$ by changing the time-dependent oscillation energy to the time-independent one as $\varepsilon_d(t) \to E_d$, and hence the coupling strengths become time-dependent

$$R_{\gamma k} \to \widetilde{R}_{\gamma k}(t) = R_{\gamma k}\exp\Big[-i\sum_{j=1}^{2}\lambda_j\sin(\omega_j t)\Big]. \quad (2)$$

The terminals are considered as macroscopic electron reservoirs which are described by the grand canonical ensembles when the terminals are uncoupled from the central region. The current noise is determined by the current fluctuation correlation as

$$\Pi_{\gamma\gamma'}(t,t') = \langle\delta\hat{I}_\gamma(t)\delta\hat{I}_{\gamma'}(t')\rangle + \langle\delta\hat{I}_{\gamma'}(t')\delta\hat{I}_\gamma(t)\rangle, \quad (3)$$

where $\delta\hat{I}_\gamma(t) = \hat{I}_\gamma(t) - \langle\hat{I}_\gamma(t)\rangle$ is the current fluctuation operator. The symbol $\langle ...\rangle$ in above formula denotes the quantum expectation over the electron state, and ensemble average over the system. In order to obtain the noise spectrum, we have to know the current operators in the terminals. According to the continuity equation and Heisenberg equation, we can find the operator of current flowing into the QD from the γth lead. The current operator of the γth lead is expressed as

$$\hat{I}_\gamma(t) = -\frac{ie}{\hbar}\sum_{k\sigma}\Big[\widetilde{R}_{\gamma k}^*(t)d_\sigma^\dagger(t)a_{\gamma,k\sigma}(t) - \text{H.C.}\Big]. \quad (4)$$

For the coupled system, the electron operators $d_\sigma^\dagger(t)$ and $a_{\gamma,k\sigma}(t)$ are coupled to each other, and they are in nonequilibrium state under the applied fields and source-drain bias. In order to express the operator $d_\sigma^\dagger(t)$ in terms of $a_{\gamma,k\sigma}^\dagger(t)$, we employ the equation of motion method to derive the separate operators self-consistently, and then express the electron operators by the equilibrium electron operators of terminals as the different parts of the system are uncoupled. The electron operators can also be related to the retarded and advanced Green's functions of the coupled QD. The coupled annihilation operator of electron in the γth lead can be derived from the Heisenberg equation as

$$a_{\gamma,k\sigma}(t) = \int dt_1 g_{\gamma,k}^r(t,t_1)\widetilde{R}_{\gamma k}(t_1)d_\sigma(t_1) + \hat{a}_{\gamma,k\sigma}(t), \quad (5)$$

where $\hat{a}_{\gamma,k\sigma}(t)$ is the uncoupled annihilation operator of electron in the γth lead as there is no tunneling at the initial time t_0. We refer it as $\hat{a}_{\gamma,k\sigma}(t) = e^{-\frac{i}{\hbar}E_{\gamma,k}(t-t_0)}\hat{a}_{\gamma,k\sigma}(t_0)$ in the Heisenberg representation. The Fermi distribution function $f(E_{\gamma,k})$ is given by taking the grand canonical ensemble as $\langle\hat{a}_{\gamma,k\sigma}^\dagger\hat{a}_{\gamma',k'\sigma'}\rangle = f(E_{\gamma,k})\delta_{\gamma\gamma'}\delta_{kk'}\delta_{\sigma\sigma'}$. In equation (5), $g_{\gamma,k}^r(t,t_1)$ is the retarded Green's function of electron in the γth lead without connecting to the QD. The coupled electron operator of QD is derived through equation of motion as

$$d_\sigma(t) = \int dt_1 g_d^r(t,t_1)\sum_{\gamma k}\widetilde{R}_{\gamma k}^*(t_1)a_{\gamma,k\sigma}(t_1) + \hat{d}_\sigma(t), \quad (6)$$

where $\hat{d}_\sigma(t)$ is the uncoupled annihilation operator of electron in the QD as there is no tunneling at the initial time t_0. We refer it as $\hat{d}_\sigma(t) = e^{-\frac{i}{\hbar}E_d(t-t_0)}\hat{d}_\sigma(t_0)$ in the Heisenberg representation. $g_d^r(t,t')$ is the retarded Green's function of the isolated QD in the absence of external MWFs. To proceed, we define the retarded (advanced) Green's function of the coupled QD by $G_d^{r(a)}(t,t')$. Substituting the operator $a_{\gamma,k\sigma}$ given in equation (5) into the operator $d_\sigma(t)$ stated in equation (6), and employing the iteration procedure, we obtain the electron operator of QD expressed by the coupled Green's function of the QD as

$$d_\sigma(t) = \int dt_1 G_d^r(t,t_1)\sum_{\gamma k}\widetilde{R}_{\gamma k}^*(t_1)\hat{a}_{\gamma,k\sigma}(t_1). \quad (7)$$

We have omitted the equilibrium operator of QD $\hat{d}_\sigma(t)$ in the above formula since it has no contribution to the tunneling current. The retarded Green's function G_d^r is determined by the Dyson equation in the presence of MWFs.

Because we are interested in the multi-photon behaviors of tunneling current noise caused by MWFs, we consider the wideband limit in the two leads. Substituting the obtained electron operators into the current operator expressed in equation (4), and employing the property of Bessel functions of the first kind $J_n(\lambda)$ with the arguments λ

$$e^{-i\lambda\sin(\omega t)} = \sum_{n=-\infty}^{\infty}J_n(\lambda)e^{-in\omega t},$$

through straightforward derivation we find that the current operator can be written in the following form

$$\hat{I}_\gamma(t) = \frac{e}{h}\sum_{\beta\beta_1\sigma}\sum_{\{n_j,m_j\}}\int d\epsilon_1 d\epsilon_2\prod_{j=1}^{2}J_{n_j}(\lambda_j)J_{m_j}(\lambda_j) \times \Gamma_{\beta\beta_1}e^{\frac{i}{\hbar}[\epsilon_1-\epsilon_2+\Omega_{\{\tilde{n},\tilde{m}\}}\hbar]t}A^\gamma_{\beta\beta_1,\{\tilde{n},\tilde{m}\}}(\epsilon_1,\epsilon_2) \times \hat{a}_{\beta\sigma}^\dagger(\epsilon_1)\hat{a}_{\beta_1\sigma}(\epsilon_2), \quad (8)$$

where $\{n_j, m_j\} = n_1, m_1, n_2, m_2$ are integers ranging from $-\infty$ to ∞. In the formula, $\hat{a}_{\beta\sigma}^\dagger(\epsilon_1)$ and $\hat{a}_{\beta_1\sigma}(\epsilon_2)$ are electron operators of terminals β and β_1 at different energies ϵ_1 and ϵ_2 in equilibrium state as the different subsystems are disconnected from each other. The coefficient $A^\gamma_{\beta\beta_1,\{\tilde{n},\tilde{m}\}}(\epsilon_1,\epsilon_2)$ is defined as

$$A^\gamma_{\beta\beta_1,\{\tilde{n},\tilde{m}\}}(\epsilon_1,\epsilon_2) = i\delta_{\beta\gamma}G_d^r(\epsilon_2 - w_{\{\tilde{m}\}}) - i\delta_{\beta_1\gamma}G_d^a(\epsilon_1 - w_{\{\tilde{n}\}}) - \Gamma_\gamma G_d^a(\epsilon_1 - w_{\{\tilde{n}\}})\times G_d^r(\epsilon_2 - w_{\{\tilde{m}\}}).$$

Since the summation $\sum_{j=1}^{2} m_j\omega_j$ appears in the formulas simultaneously, we have introduced the notations $\Omega_{\{\tilde{n},\tilde{m}\}}$ and $w_{\{\tilde{m}\}}$ for writing the formulas concisely as $\Omega_{\{\tilde{n},\tilde{m}\}} = \sum_{j=1}^{2}(m_j - n_j)\omega_j$ and $w_{\{\tilde{m}\}} = \hbar\sum_{j=1}^{2} m_j\omega_j$. One should understand these notations as entire symbols relating to the integers m_j and n_j by the corresponding indices $\tilde{m}$ and $\tilde{n}$. We employ these notations also in the following formulas, and we have $\Omega_{\{\tilde{n},\tilde{m}\}} = -\Omega_{\{\tilde{m},\tilde{n}\}}$, $w_{\{\tilde{n}\}} = \hbar\sum_{j=1}^{2} n_j\omega_j$. In addition, the following reality relation holds $A^{\gamma}_{\beta\beta_1,\{\tilde{n},\tilde{m}\}}(\epsilon_1,\epsilon_2)^* = A^{\gamma}_{\beta_1\beta,\{\tilde{m},\tilde{n}\}}(\epsilon_2,\epsilon_1)$. The Fourier transformed Green's functions of the central dot is determined by the Fourier transformed Dyson equation from which one can find the retarded and advanced Green's functions. $\Gamma_{\beta\beta_1}$ is the line-width function of terminals in the wideband limit defined by $\Gamma_{\beta\beta_1}(\epsilon) = 2\pi\sum_k R^*_{\beta k}R_{\beta_1 k}\delta(\epsilon - E_{\beta,k})$. The lifetime of the system is $\tau_0 = 2/\Gamma(\epsilon)$, where $\Gamma(\epsilon) = \Gamma_L(\epsilon) + \Gamma_R(\epsilon)$, and $\Gamma_\beta(\epsilon) = \Gamma_{\beta\beta}(\epsilon)$. The retarded (advanced) Green function of the QD is found to be $G_d^{r(a)}(\epsilon) = (\epsilon - E_d \pm \frac{i}{2}\Gamma)^{-1}$ in the wideband limit. In the presence of ac fields, there exist infinite channels in the QD for electrons in the terminals to transport.

The current of γth lead is given by taking quantum average over the compound quantum state and ensemble average, $I_\gamma(t) = \langle\hat{I}_\gamma(t)\rangle$. By employing the Fermi distribution function of electrons $f_\gamma(\epsilon)$ in the terminals, direct derivation results in the time-evolving current tunneling from the γth lead to the QD as

$$I_\gamma(t) = \frac{2e}{h}\sum_{\beta}\sum_{\{n_j,m_j\}}\int d\epsilon\prod_{j=1}^{2} J_{n_j}(\lambda_j)J_{m_j}(\lambda_j)\Gamma_\beta \times e^{i\Omega_{\{\tilde{n},\tilde{m}\}}t}A^{\gamma}_{\beta\beta,\{\tilde{n},\tilde{m}\}}(\epsilon,\epsilon)f_\beta(\epsilon). \quad (9)$$

The time-dependent current contains contributions from the diagonal ($n_j = m_j$) terms and off-diagonal ($n_j \neq m_j$) terms. The off-diagonal components oscillate with time, which represents the processes of nonequal absorption and emission of photons from the jth field. The applied MWFs can be divided into two kinds : (a) the two angular frequencies ω_1 and ω_2 are independent on each other, which is referred as the incommensurate case; (b) the two frequencies possess the relation $\omega_2/\omega_1 = q$ with q being an integer, which is referred as the commensurate case. For case (a), the time-averaged net tunneling current I is obtained simply by letting $m_j = n_j$ in the current formula (9), and tunneling current is determined by the transmission coefficient of electron $T_{\gamma\gamma'}(\epsilon)$ by the Landauer-Büttiker-like formula [45]. In the absence of external ac fields, the transmission coefficient of electron tunneling from the γ' terminal to the γth terminal is defined by $T_{\gamma\gamma'}(\epsilon) = \Gamma_\gamma\Gamma_{\gamma'} \mid G_d^r(\epsilon) \mid^2$. For the commensurate case, the time-averaged current is given by setting the subscripts under the restriction $n_1 = m_1 + (m_2 - n_2)q$ to give the time averaged current in the γth terminal

$$I_\gamma = \frac{2e}{h}\sum_{\beta}\sum_{m_1m_2n_2}\int d\epsilon J_{m_1}(\lambda_1)J_{m_1+(m_2-n_2)q}(\lambda_1) \times J_{m_2}(\lambda_2)J_{n_2}(\lambda_2)T_{\gamma\beta}(\epsilon - w_{\{\tilde{m}\}})\Big[f_\gamma(\epsilon) - f_\beta(\epsilon)\Big]. \quad (10)$$

The current conservation $\sum_\gamma I_\gamma = 0$ is satisfied in the above formula. This current formula is equivalent to the one derived from the approach of Jauho, Wingreen, and Meir by employing the Keldysh Green's function [41].

Substituting the current operator given in equation (8) into the current fluctuation correlation formula defined by equation (3), we encounter four electron operator correlations related to the equilibrium state of electrons in the terminals. The four electron operator correlations can be written into the products of two pair-electron correlations from the Wick's theorem. This treatment results in the current fluctuation correlation function

$$\Pi_{\gamma\gamma'}(t,t') = 2\Big(\frac{e}{h}\Big)^2\sum_{\beta\beta_1}\sum_{\{n_j,m_j\}}\sum_{\{n'_j,m'_j\}}\int d\epsilon_1 d\epsilon_2 \times\prod_{j=1}^{2} J_{n_j}(\lambda_j)J_{m_j}(\lambda_j)J_{n'_j}(\lambda_j)J_{m'_j}(\lambda_j)\Gamma_\beta\Gamma_{\beta_1} \times e^{\frac{i}{\hbar}(\epsilon_1-\epsilon_2)(t-t')}e^{i[\Omega_{\{\tilde{n},\tilde{m}\}}t+\Omega_{\{\tilde{n}',\tilde{m}'\}}t']} \times A^{\gamma}_{\beta\beta_1,\{\tilde{n},\tilde{m}\}}(\epsilon_1,\epsilon_2)A^{\gamma'}_{\beta_1\beta,\{\tilde{n}',\tilde{m}'\}}(\epsilon_2,\epsilon_1) \times F_{\beta\beta_1}(\epsilon_1,\epsilon_2), \quad (11)$$

where $\{n_j,m_j\} = n_1,n_2,m_1,m_2$; $\{n'_j,m'_j\} = n'_1,n'_2,m'_1,m'_2$; $w_{\{\tilde{m}'\}} = \hbar\sum_{j=1}^{2} m'_j\omega_j$. The summations over the integers $n_1,n_2,m_1,m_2,n'_1,n'_2,m'_1,m'_2$ range from $-\infty$ to ∞. The function $F_{\beta\beta_1}(\epsilon,\epsilon_1)$ in the above formula is defined from the equilibrium features of the electron reservoirs associated with the Fermi distribution functions $f_\beta(\epsilon)$ by the form $F_{\beta\beta_1}(\epsilon,\epsilon_1) = f_\beta(\epsilon)[1 - f_{\beta_1}(\epsilon_1)] + f_{\beta_1}(\epsilon_1)[1 - f_\beta(\epsilon)]$. This function satisfies the relation $F_{\beta\beta_1}(\epsilon,\epsilon_1) = F_{\beta_1\beta}(\epsilon_1,\epsilon)$. The correlation function given in equation (11) describes the current correlation evolution procedure related to the two times t and t'. The time-evolution is strongly dependent on the quantities $\Omega_{\{\tilde{n},\tilde{m}\}}$ and $\Omega_{\{\tilde{n}',\tilde{m}'\}}$, which are composed of different ac fields. This correlation function is real, i.e., $\Pi_{\gamma\gamma'}(t,t') = \Pi_{\gamma\gamma'}(t,t')^*$, which can be seen by taking the transformation over the subscripts as $n_j \to m_j$, $n'_j \to m'_j$, and then by replacing the arguments ϵ_1 and ϵ_2 in the Fourier space. We exchange the terminal indices β and β_1, by employing the symmetry relation of $F_{\beta\beta_1}(\epsilon,\epsilon_1)$, and comparing the quantity $\Pi_{\gamma\gamma'}(t,t')$ with its complex conjugate $\Pi_{\gamma\gamma'}(t,t')^*$ by employing the reality relation of $A^{\gamma}_{\beta\beta_1,\{\tilde{n},\tilde{m}\}}(\epsilon_1,\epsilon_2)$. Therefore one finds that the correlation function is real. From the definition of spectral density of shot noise $\frac{1}{2\pi}\Pi_{\gamma\gamma'}(\Omega,\Omega') = S_{\gamma\gamma'}(\Omega)\delta(\Omega+\Omega')$, where Ω and Ω' are the frequencies associated with the Fourier transformation over times t and t', one obtains the noise formula by making Fourier transformation over

equation (11)

$$S_{\gamma\gamma'}(\Omega) = \frac{2e^2}{h}\sum_{\beta\beta_1}\sum_{\{n_j,m_j\}}\sum_{\{n'_j,m'_j\}}\int d\epsilon \prod_{j=1}^{2} J_{n_j}(\lambda_j) \times J_{m_j}(\lambda_j)J_{n'_j}(\lambda_j)J_{m'_j}(\lambda_j)A^{\gamma}_{\beta\beta_1,\{\tilde{n},\tilde{m}\}}(\epsilon,\widetilde{\epsilon}_{\{\tilde{n},\tilde{m}\}}) \times \Gamma_\beta\Gamma_{\beta_1}A^{\gamma'}_{\beta_1\beta,\{\tilde{n}',\tilde{m}'\}}(\widetilde{\epsilon}_{\{\tilde{n},\tilde{m}\}},\epsilon)F_{\beta\beta_1}(\epsilon,\widetilde{\epsilon}_{\{\tilde{n},\tilde{m}\}}). \quad (12)$$

We have defined the argument in the formula as $\widetilde{\epsilon}_{\{\tilde{n},\tilde{m}\}} = \epsilon + \hbar\Omega_{\{\tilde{n},\tilde{m}\}} + \hbar\Omega$. The energy conservation for the electron absorption and emission of photons during the electron tunneling procedure requires the constraint $\Omega_{\{\tilde{n},\tilde{m}\}} + \Omega_{\{\tilde{n}',\tilde{m}'\}} = 0$. This condition results in the selection rule for the numbers associated with absorption and emission of photons as $m_1 - n_1 + (m_2 - n_2)q + m'_1 - n'_1 + (m'_2 - n'_2)q = 0$, where q is ratio of the two frequencies as $q = \omega_2/\omega_1$. The situations for photon absorption and emission are quite different for the commensurate and incommensurate MWFs. The spectral density of shot noise can be written in terms of the transmission coefficient by substituting the relation $A^{\gamma}_{\beta\beta_1,\{\tilde{n},\tilde{m}\}}(\epsilon,\epsilon')$ defined by equation (8) into the noise formula equation (12). Specifically, we consider the spectral density of noise at $\Omega = 0$, and finally we arrive at the following expression

$$S_{\gamma\gamma}(0) = \frac{4e^2}{h}\sum_{\{n_j,m_j\}}\sum_{\{n'_j,m'_j\}}\int d\epsilon \prod_{j=1}^{2} J_{n_j}(\lambda_j) \times J_{m_j}(\lambda_j)J_{n'_j}(\lambda_j)J_{m'_j}(\lambda_j)T_{\gamma\gamma'}(\epsilon - w_{\{\tilde{n}\}}) \times T_{\gamma\gamma'}(\epsilon - w_{\{\tilde{m}'\}})\Big\{\frac{1}{2}\sum_{\beta}F_{\beta\beta}(\epsilon,\widetilde{\epsilon}_{\{\tilde{n},\tilde{m}\}}) + Y_{\{\tilde{n}\},\{\tilde{m}'\}}(\epsilon)F_{\gamma\gamma'}(\epsilon,\widetilde{\epsilon}_{\{\tilde{n},\tilde{m}\}})\Big\}, \quad (13)$$

for $\gamma \neq \gamma'$, $(\gamma,\gamma' \in \{L,R\})$. In the above formula, we have defined the function as $Y_{\{\tilde{n}\},\{\tilde{m}'\}}(\epsilon) = [(\epsilon - w_{\{\tilde{n}\}} - E_d)(\epsilon - w_{\{\tilde{m}'\}} - E_d) + \frac{1}{4}\Gamma^2]/(\Gamma_\gamma\Gamma_{\gamma'}) - 1$. The first term containing the function $F_{\beta\beta}(\epsilon,\widetilde{\epsilon}_{\{\tilde{n},\tilde{m}\}})$ represents the thermal noise perturbed by the ac fields, which in general deviates from the equilibrium noise. According to the selection rule, there exist different processes for electrons to absorb and emit photons, and therefore we have different forms of spectral density of noise. The second term containing the function $F_{\gamma\gamma'}(\epsilon,\widetilde{\epsilon}_{\{\tilde{n},\tilde{m}\}})$, $\gamma \neq \gamma'$, describes the photon-assisted shot noise induced by both of the dc and ac biases. Under the perturbation of MWFs, the electrons tunneling in the channels $\epsilon = w_{\{\tilde{n}\}} + E_d$ interfere with the electrons tunneling in the channels $\epsilon = w_{\{\tilde{m}'\}} + E_d$. However, the strengths of interference are weighted by the Bessel functions corresponding to these channels. The concrete forms of the Bessel functions are also dependent on the selection rule self-consistently. In the absence of the MWFs, the noise spectral density reduces to the previously known noise formula [25], which is zero as the source-drain bias is removed at zero temperature. However, under the perturbation of MWFs, the noise is intimately dependent on the matching-mismatching of side-bands of the ac fields. If two side-bands related to different MWFs overlap, further splitting of electron energy in the QD may cause shifting of tunneling channels. Consequently, the enhancement or suppression of shot noise may be generated due to the way of fields application and controlling of external mechanism. In the follows, we examine the absorption and emission processes for the commensurate and incommensurate MWFs concerning the noise spectral density of the left terminal by $S = S_{LL}(0)$.

2.1 Incommensurate MWFs perturbation

For the incommensurate case, the frequency ratio q can be any real number except integer. From the electron-photon selection rule there are two possibilities for the numbers of photon absorption and emission: one is the incommensurate unbalanced case and the other is the incommensurate balanced case.

For the balanced absorption and emission process, the numbers reduced from the selection rule are restricted by $m_2 = n_2$, $m'_2 = n'_2$, and $m_1 = n_1, m'_1 = n'_1$, which is the pseudo-equilibrium procedure. This procedure indicates that the absorbed and emitted photons from the ith MWF are conserved. This means that the photons with the frequency ω_i of the ith field irradiating to the QD keep the same number of photons with the same frequency after emission from the QD. The noise spectral density for the incommensurate balanced case derived from equation (13) takes the form by letting the subscripts of the Bessel functions according to the above selection rule. Therefore, the product of 8 Bessel function becomes $J^2_{n_1}(\lambda_1)J^2_{n'_1}(\lambda_1)J^2_{n_2}(\lambda_2)J^2_{n'_2}(\lambda_2)$. In this case, the noise formula provides symmetric noise spectral density, and the term related to thermal noise becomes zero as the temperature approaches zero. The second term is nonequilibrium noise which is nonzero at zero temperature, but it goes to zero as the source-drain bias eV approaches zero at zero temperature. The effect of external MWFs relates to the symmetric photon-assisted tunneling, and the symmetric modification of noise resonant peaks. The stair-like shot noise is intimately related to the properties of the concrete value of the real q.

The noise formula for the unbalanced absorption case can be written out by considering the frequency ratio q being arbitrary real for the incommensurate MWFs perturbation procedure according to the selection rule. This case is associated with the nonequilibrium unbalanced absorption and emission of photons. Different from the balanced case, the unbalanced photon absorption and emission are governed by the restriction as $n'_1 = m_1 - n_1 + m'_1$ and $n'_2 = m_2 - n_2 + m'_2$ in equation (13). The quantity q does not involves in the numbers of photon absorption and emission, but it modifies the levels of QD through the side-bands induced by the external MWFs. Since the two fields possess no relation with each other, the levels of

side-bands do not overlap with each other. These incommensurate MWFs give rise to the kind of noise spectral density deviated from the pseudo-equilibrium situation by imposing the photon energies in the Fermi distribution functions. This behavior indicates that the absorbed and emitted photon energies induce bias, which drives the electrons tunneling through the system. The correlations among the photon-assisted tunneling currents are nonzero even if in the absence of source-drain bias eV at zero temperature.

2.2 Commensurate MWFs perturbation

When the frequency ratio q of the two external MWFs is an integer, the channels of the side-bands may overlap with each other, and the perturbations of two commensurate fields cause novel behaviors. In this case, the channels and Bessel functions are related to the frequency ratio number (commensurate number) q, which leads to complete novel behaviors associated with the balanced and unbalanced absorptions of MWFs.

For the commensurate balanced absorption case, there exists a pseudo-equilibrium balanced absorption process according to the electron-photon selection rule that $n_1 = m_1 + (m_2 - n_2)q, n_1' = m_1' + (m_2' - n_2')q$. The perturbation of the two fields causes asymmetric side-bands weighted with Bessel function. For this case, the absorbed photons in one channel branch of current may be emitted to the other channel branches. The conservation of the photon energy and the correlation among branches of current lead to the noise formula

$$S = \frac{4e^2}{h} \sum_{m_1 m_2 n_2} \sum_{m_1' m_2' n_2'} \int d\epsilon J_{m_1+(m_2-n_2)q}(\lambda_1) J_{m_1}(\lambda_1) \times J_{m_1'+(m_2'-n_2')q}(\lambda_1) J_{m_1'}(\lambda_1) J_{n_2}(\lambda_2) J_{m_2}(\lambda_2) \times J_{n_2'}(\lambda_2) J_{m_2'}(\lambda_2) T_{LR}(\epsilon - w_{\{\tilde{m}\}}) T_{LR}(\epsilon - w_{\{\tilde{m}'\}}) \times \left\{ \frac{1}{2} \sum_{\beta} F_{\beta\beta}(\epsilon, \epsilon) + Y_{\{\tilde{m}\},\{\tilde{m}'\}}(\epsilon) F_{LR}(\epsilon, \epsilon) \right\}. \quad (14)$$

This balanced absorption case gives quite different noise structure compared with the corresponding case for the incommensurate fields perturbation. The common properties for the two balanced cases is that at zero source-drain bias, the shot noise becomes zero when the temperature approaches zero. However, the asymmetric behavior aroused from the perturbation of commensurate fields contains more physical connotations in equation (14).

For the commensurate unbalanced absorption case, there exists an unbalanced absorption according to the electron-photon selection rule for the photon absorption and emission numbers. The perturbation of external fields makes the noise spectral density being nonequilibrium, and the selection rule of the current noise is given by $n_1' = m_1 - n_1 + m_1' + (m_2 - n_2 + m_2' - n_2')q$. In this case, the noise spectrum is derived from equation (13) that

$$S = \frac{4e^2}{h} \sum_{n_1, n_2} \sum_{m_1, m_2} \sum_{m_1' m_2' n_2'} \int d\epsilon J_{n_1}(\lambda_1) J_{m_1}(\lambda_1) J_{m_1'}(\lambda_1) \times J_{m_1 - n_1 + m_1' + (m_2 - n_2 + m_2' - n_2')q}(\lambda_1) J_{n_2}(\lambda_2) \times J_{m_2}(\lambda_2) J_{n_2'}(\lambda_2) J_{m_2'}(\lambda_2) T_{LR}(\epsilon - w_{\{\tilde{n}\}}) \times T_{LR}(\epsilon - w_{\{\tilde{m}'\}}) \Big\{ \frac{1}{2} \sum_{\beta} F_{\beta\beta}(\epsilon, \tilde{\epsilon}_{\{\tilde{n},\tilde{m}\}}) + Y_{\{\tilde{n}\},\{\tilde{m}'\}}(\epsilon) F_{LR}(\epsilon, \tilde{\epsilon}_{\{\tilde{n},\tilde{m}\}}) \Big\}. \quad (15)$$

The case of commensurate unbalanced absorption possesses the property of both heavy asymmetric structure of noise and the nonequilibrium behavior of current correlation. Multi-channel correlation associated with the side-bands indicates multi-photon absorption and emission procedure. The noise is nonzero as the source-drain bias is removed at zero temperature. Both of the thermal noise and shot noise terms contribute to nontrivial noise spectrum, and the overlapping circumstance may cause novel noise behaviors in the nonlinear regime of applied MWFs.

3 Numerical calculations

In this section we present the numerical calculations and examine the behaviors of shot noise and differential shot noise at zero temperature. We are interested in the situation that the system is perturbed by the commensurate MWFs, in which the shot noise is associated with the commensurate balanced photon absorption procedure shown by equation (14), and the commensurate unbalanced photon absorption procedure determined by equation (15). As two MWF's are applied to the QD, the current splits to form many branches. The different branch electron tunneling interference gives rise to total current. We deal with the spin degenerate case because the system is not affected by magnetic fields. The chemical potential of the right lead μ_R is taken as the reference of energy in different parts. E_d is the measured energy of QD, which can be expressed by the gate voltage V_g as $E_d = E_0 + eV_g$, and we set $E_0 = 0$ without loss of generality. We define the scale of shot noise by $S_0 = 4e^2\Delta/h$, where the photon energy of one field $\Delta = \hbar\omega_1$ is taken as the energy measurement scale. At zero temperature, the thermal noise becomes zero, and only the shot noise remains due to the presence of source-drain bias and the perturbations of ac fields. The symmetric coupling system $\Gamma_L = \Gamma_R = \Gamma/2$ is considered throughout the numerical calculations. To apply the free electron single-level QD model experimentally, the frequencies of the imposed signals should be restricted in order not to cause level crossing due to the applied fields. The frequencies can be chosen from the radio frequency (RF) (about 1MHz) to the microwave frequency (about 40 GHz) for a relatively large QD. Such system is composed by the etched narrow wire with width 0.8 μ

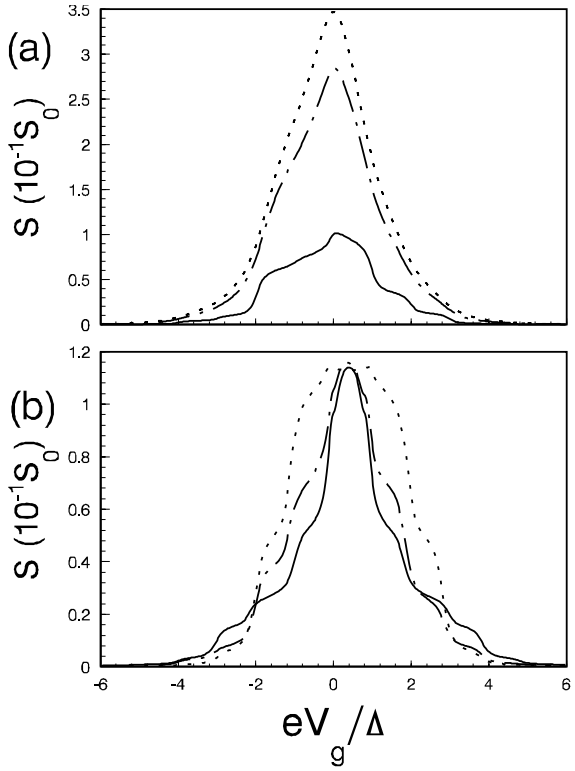

Fig. 1. The shot noise S versus gate voltage for the commensurate unbalanced absorption. In diagram (a), we show the behaviors of noise as $q = 2$, and $\lambda_1 = \lambda_2 = 0.8$. The solid, dotted, and dash-dotted curves are related to the parameters $\Gamma = 0.2\Delta$, $\Gamma = 0.8\Delta$, $\Gamma = 0.6\Delta$ correspondingly at $eV = 0$. Diagram (b) displays the characteristics of the shot noise as $\Gamma = 0.2\Delta$, and $eV = 0.8\Delta$. The other parameters are chosen as $\lambda_1 = \lambda_2 = 0.8, q = 2$ for the dash-dotted curve;$\lambda_1 = 0.8, \lambda_2 = 1.6, q = 1$ for the dotted curve; $\lambda_1 = 0.8, \lambda_2 = 1.6/3, q = 3$ for the solid curve.

widening into source and drain 2DEG region, which contains roughly 100 electrons and is weakly coupled to the source and drain [1,14]. The charging energy is usually in the regime as $U \approx 0.2 \sim 2$ meV. However, for a relatively small QD with the two-dimension confined in the regime about 70 nm, the level space between the first level to the bottom of the QD is about 0.5 meV. The Coulomb interaction $U \approx 2.7$ meV. Such small QD contains about 20 electrons [46]. In this paper, we choose the photon energy $\Delta = \hbar\omega_1$ as the measurement energy scale, and we take it as $\Delta = 0.02$ meV, (frequency $\nu \approx 4.85$ GHz). Other energy quantities are compared with it, and the nonlinear effects are involved in the system by taking the energy regime of the other quantities as $0 \sim 10\Delta$. We assume the magnitudes of the ac fields possess the relation $eV_2 = 2eV_1$, so that the arguments of the Bessel functions $\lambda_i (i = 1, 2)$ are given by $\lambda_1 = eV_1/\Delta$, and $\lambda_2 = 2\lambda_1/q$. In the numerical calculations we take the line-width $\Gamma < \Delta$, which is in the nonadiabatic regime of the mesoscopic tunneling.

Figure 1 displays the resonance of shot noise versus gate voltage V_g under the perturbation of commensurate MWFs for the unbalanced case. The asymmetric behaviors of the shot noise in Figure 1a show the absorption and emission of photons as the two commensurate fields irradiate to the QD in the absence of source-drain bias eV. This signifies that the numbers of photon absorption and emission are not equal, which means the absorbed photons from one field may be emitted to the other field. The detailed resonant behaviors are strongly related to the line-width of the system, and the asymmetry is more evidently shown in the obvious quantum regime as $\Gamma \ll \Delta$. The magnitude of shot noise is larger with a larger magnitude of line-width Γ. This kind of shot noise is contributed by purely photon absorption effect, in which both of the photon induced terminal fluctuation and photon-electron pumping effect play important roles. This shows that shot noise is strongly dependent on the ac fields, however the time-averaged tunneling current is zero in the absence of source-drain bias whenever the ac fields are applied through the gate of QD. Several steps displayed in each side of the resonant peak indicate the multi-photon absorption and emission processes. Since the spectral density of shot noise is constructed from the correlations of two currents at different times, the absorbed photons carried by one of the currents will be emitted to the other current due to the current correlation according to the selection rule. For the commensurate MWFs perturbed system, the selection rule is governed by the frequencies of the commensurate fields stated by the integer q. Therefore, different commensurate number q contributes to different photon absorption and emission processes, and we obtain different resonant structures of shot noise shown in Figure 1b. The switching on of source-drain bias suppresses the magnitude of shot noise, but it strengthens the symmetric structure of the shot noise. The commensurate number q does not affect the magnitude of the shot noise obviously.

We show the variation of shot noise with respect to the source-drain bias eV for the commensurate unbalanced photon absorption and emission processes in Figure 2. The shot noise exhibits symmetric inverse resonant behavior versus source-drain bias eV in the absence of MWFs shown by the dotted curve in Figure 2a. It is zero as $eV = 0$, and it increases to its saturated value $0.3S_0$ by increasing the absolute value of the source-drain voltage. This behavior shows the nonequilibrium feature of shot noise. As we apply a single MWF on the QD, the shot noise is nonzero due to the photon-assisted current correlations (solid curve). This kind of noise has been discussed by Büttiker et al. in references [8,25]. It should be pointed out that as MWFs apply to the QD system through its gate, the time-averaged tunneling current is zero in the absence of source-drain bias since the photon pumped electrons from the QD to the two leads are equal. The nonzero shot noise arises from the current correlation of unbalanced absorption and emission processes. For the double commensurate MWFs applied system, the shot noise is large enough to surpass its saturated value due to the unbalanced absorption and emission procedures (dash-dotted curve). We depict the shot noise with respect to the source-drain bias under the perturbation of two

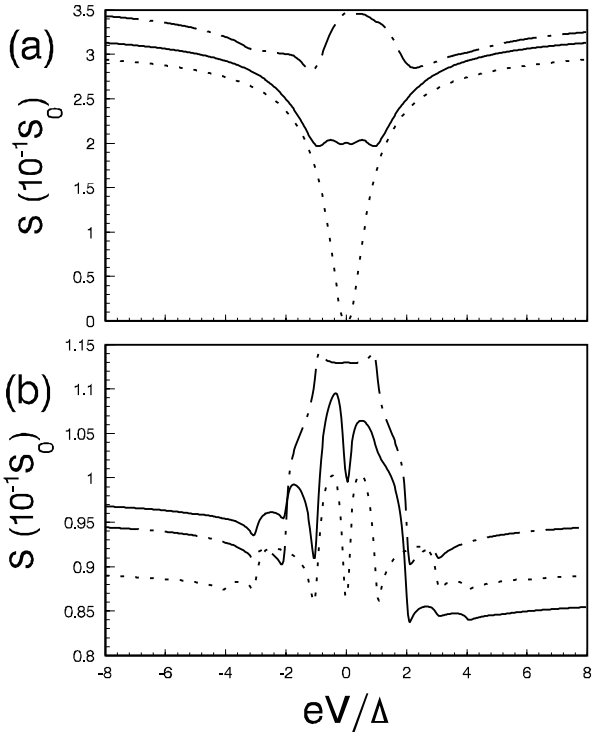

Fig. 2. The shot noise S versus source-drain bias eV as $eV_g = 0$. In diagram (a), the parameters are chosen as $\Gamma = 0.8\Delta$, and the dash-dotted curve is associated with $\lambda_1 = \lambda_2 = 0.8$, $q = 2$ for the commensurate unbalanced case; the solid curve is associated with $\lambda_1 = 0.8, \lambda_2 = 0$ for the single field applied system; the dotted curve corresponds to $\lambda_1 = \lambda_2 = 0$. Diagram (b) shows the commensurate unbalanced case as $\Gamma = 0.2\Delta$,$\lambda_1 = 0.8$, $\lambda_2 = 2\lambda_1/q$. The dash-dotted, solid, dotted curves correspond to $q = 1, 2, 3$, respectively.

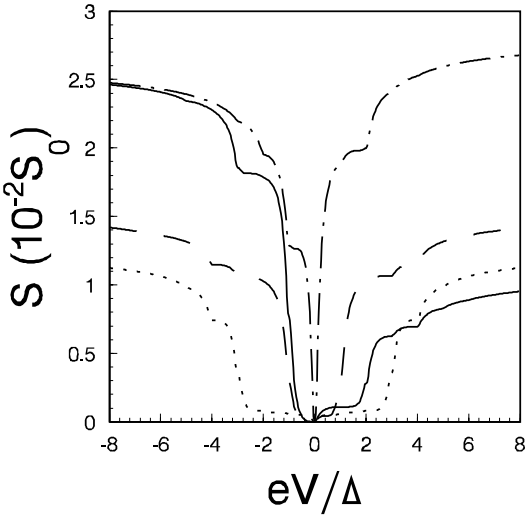

Fig. 3. The shot noise versus source-drain bias eV for the commensurate balanced case. The parameters are chosen as $\Gamma = 0.2\Delta$, $eV_g = 0$, and for the solid curve $\lambda_1 = \lambda_2 = 1.5$, $q = 2$; for the dash-dotted curve $\lambda_1 = \lambda_2 = 0.8$, $q = 2$; for the dashed curve $\lambda_1 = 1.5, \lambda_2 = 1.0$, $q = 3$; for the dotted curve $\lambda_1 = 1.5$, $\lambda_2 = 3.0$, $q = 1$.

commensurate MWFs for different commensurate number q in Figure 2b as the line-width $\Gamma = 0.2\Delta$, which is in the nonadiabatic regime. The shot noise contains reach structure as the source-drain bias is small $\mid eV \mid < 4\Delta$, and the detailed photon-assisted behaviors disappear when the source-drain bias becomes large enough $\mid eV \mid > 4\Delta$. The quantum behaviors induced by the photon absorption and emission become more evident with a smaller Γ. The dash-dotted curve represents the shot noise as $q = 1$, which is much larger around $eV = 0$ than that of the saturated value when $\mid eV \mid > 4\Delta$. One observes that the shot noise is split as $q = 2$, and the splitting becomes heavier when $q = 3$. This situation is associated with the inverse resonance of photon channel suppression, and the positions of suppression valleys are located at absorbed and emitted photon energies $n\Delta$.

The behaviors of shot noise for the commensurate balanced absorption and emission procedure is displayed in Figure 3, which appears quite differently from the commensurate unbalanced cases. The shot noise for the commensurate balanced case is zero as $eV = 0$, which is analogous to the equilibrium situation. The shot noise increases as the absolute value of source-drain bias eV increases, and stair-like behavior appears. The solid and dash-dotted curves are associated with the cases as $q = 2$ but with different λ_i. Multi-photon absorption procedure takes place as the biases of MWFs are strong ($eV_1 = 1.5\Delta, eV_2 = 3.0\Delta$), and the magnitude of the shot noise is suppressed more heavily as compensation. The asymmetric curves indicate that the property of shot noise is different in different regimes as $eV > 0$ and $eV < 0$. The number of steps is related to the absorbed and emitted multi-photon energies. As $q = 1$ and $q = 3$, $\lambda_1 = 1.5$, but with different λ_2, we find that the shot noise is suppressed to exhibit a gap which is about 4.6Δ for the case $q = 1$, and the noise approaches symmetric structure. The magnitude of shot noise strongly relies on the strengths of λ_i. The width of valley is dependent on the commensurate number q and together with λ_i. The noise gap for the case $q = 1$ indicates that the side channels $n = \pm 1, \pm 2$ have been blockaded originated from the multi-photon absorption and emission. The magnitude of shot noise at pth channel associated with the side-band $p\Delta$ is weighted by $J_p^4(\Lambda)$ according to equation (14) due to the contribution of multi-photon absorption and emission, where $\Lambda = \lambda_1 + \lambda_2$ and p is an integer related to the absorption and emission of photons. One observes that the weight is associated with $J_1^4(4.5) \approx J_2^4(4.5) \approx 2.5 \times 10^{-3}$ for the dotted curve. The noise of channel $p\Delta$ will be completely suppressed if Λ is a zero of the Bessel function $J_p(\Lambda)$. Similar channel blockade exists in the differential conductance and tunneling current, and we will discuss it later on the differential conductance.

We present the differential shot noise for the commensurate unbalanced absorption and emission case in Figure 4 to investigate the detailed structure of shot noise clearly. The Fano-like behaviors are exhibited for different commensurate number q, and the positions of peaks and

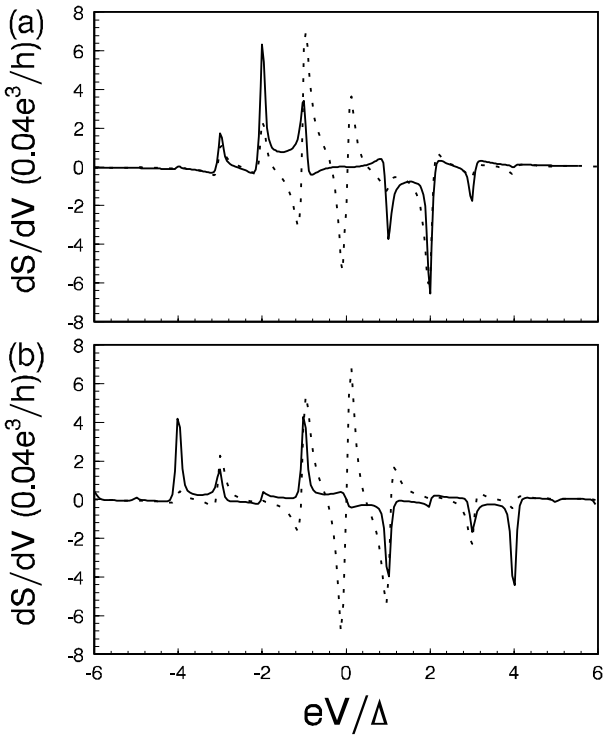

Fig. 4. The differential shot noise versus source-drain bias eV for the commensurate unbalanced case. The parameters are chosen as $\Gamma = 0.2\Delta$, $eV_g = 0$. In diagram (a), the other parameters for the solid curve are $\lambda_1 = 0.8$, $\lambda_2 = 1.6$ $q = 1$; the other parameters for the dotted curve are $\lambda_1 = \lambda_2 = 0.8$ for $q = 2$. Diagram (b) displays the curves for $q = 3$. The dotted curve is associated with $\lambda_1 = 0.8$, $\lambda_2 = 1.6/3$; the solid curve is associated with $\lambda_1 = 1.8$, $\lambda_2 = 1.2$.

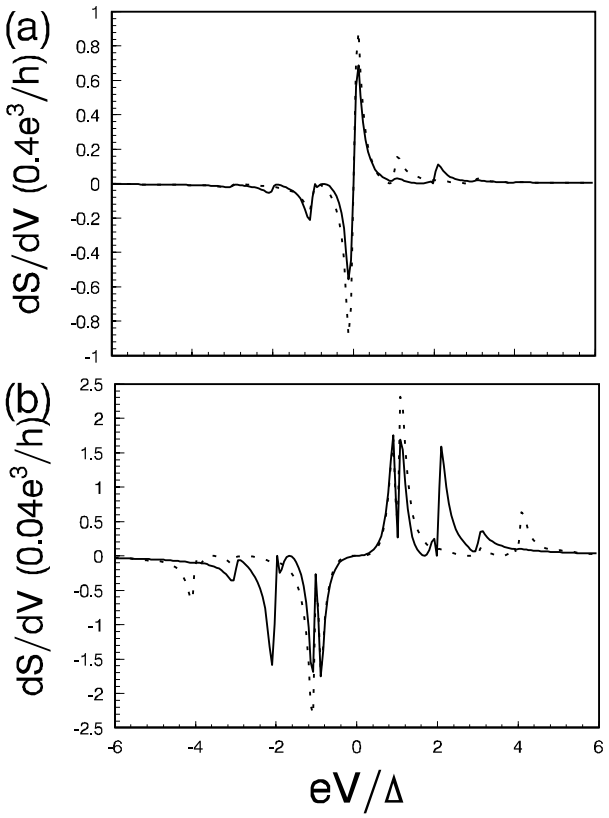

Fig. 5. The differential shot noise versus source-drain bias eV for the commensurate balanced case. The parameters are chosen as $\Gamma = 0.2\Delta$, $eV_g = 0$. Diagram (a) corresponds to $\lambda_1 = \lambda_2 = 0.8$, $q = 2$ for the solid curve; $\lambda_1 = 0.8$, $\lambda_2 = 1.6/3$, and $q = 3$ for the dotted curve. Diagram (b) corresponds to $\lambda_1 = 0.8$, $\lambda_2 = 1.6$, $q = 1$ for the solid curve; $\lambda_1 = 1.8$, $\lambda_2 = 1.2$, and $q = 3$ for the dotted curve.

valleys are located at the absorbed and emitted photon numbers related to the photon energy $n\Delta$. It is clearly recognized that the structure of different shot noise reflects the multi-photon irradiation of the two fields, and the positive-negative behaviors appear in both of the positive and negative values of eV. The Fano behavior is evidently exhibited for the cases with $q = 2, 3$ shown by the dotted curves in diagrams (a) and (b). However, this structure is smeared by increasing the magnitudes of λ_1 and λ_2 shown by the solid curve of diagram (b). We also noted that the structures of differential shot noise is quite different for case $q = 1$ from the cases for $q = 2, 3$. The central regime of dS/dV for the case $q = 1$ is related to the plateau of the dash-dotted curve in Figure 2b, while the peak-valleys of the dotted curves in Figure 4 at $eV = 0$ are related to the valleys of solid and dotted curves of Figure 2b.

The differential shot noise for the commensurate balanced absorption and emission case is depicted in Figure 5. One observes that the Fano-like peak and valley behavior is displayed around $eV = 0$. The differential shot noise dS/dV is positive as $eV > 0$, and it is negative as $eV < 0$. The multi-photon absorption and emission procedure causes the splitting of peak and valley structure. Since the magnitude of dS/dV is larger enough for $q = 2, 3$ in Figure 5a, the side structure of it is suppressed to relatively small values. As $\lambda_1 = 0.8, \lambda_2 = 1.6$, the magnitude of dS/dV is small so that the detailed structure of it is seen obviously in Figure 5b by the solid curve for q=1. The multiple peaks and valleys are related to the multi-photon assisted shot noise, and the positions of peaks and valleys are associated with the steps in the shot noise compared with Figure 3. We also present the curve for the case where $q = 3$ but with large magnitudes of λ_i shown by the dotted curve of diagram (b). One observes that the differential shot noise is suppressed by increasing the magnitudes of λ_i, and its shape is modified by increasing the fields. The smeared shot noise in the regime $eV < 0.5\Delta$ is arisen from the suppression of central channel due to the multi-photon absorption.

The differential conductance at zero temperature for the double commensurate fields applied system is given by the formula

$$\frac{dI}{dV} = G_0 \sum_{m_1 m_2 n_2} J_{m_1}(\lambda_1) J_{m_1+(m_2-n_2)q}(\lambda_1) \times J_{m_2}(\lambda_2) J_{n_2}(\lambda_2) T_{LR}(eV - w_{\{\tilde{m}\}}), \quad (16)$$

where $G_0 = 2e^2/h$. We display the differential conductance of the system perturbed by two commensurate

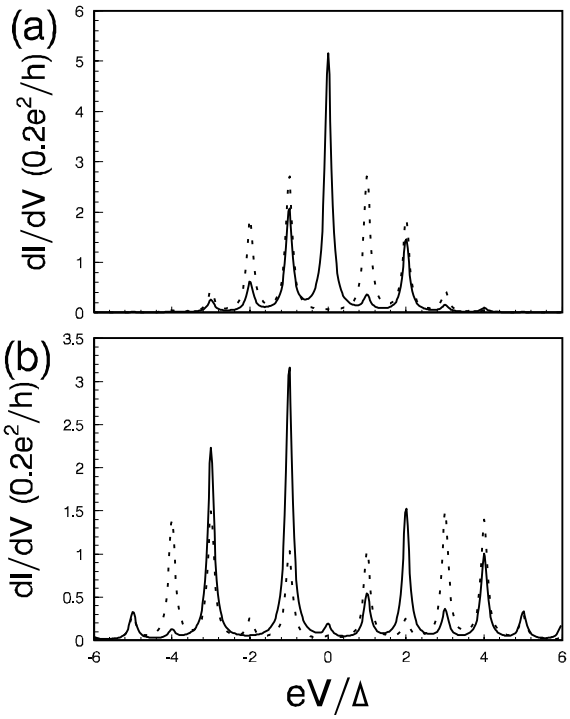

Fig. 6. The differential conductance versus source-drain bias eV for the commensurate fields applied system. The parameters are chosen as $\Gamma = 0.2\Delta$, $eV_g = 0$. In diagram (a), $\lambda_1 = \lambda_2 = 0.8$, and $q = 2$ for the solid curve; $\lambda_1 = 0.8$, $\lambda_2 = 1.6$, and $q = 1$ for the dotted curve. In diagram (b), $\lambda_1 = \lambda_2 = 1.8$, and $q = 2$ for the solid curve; $\lambda_1 = 1.8$, $\lambda_2 = 3.6$, and $q = 1$ for the dotted curve.

MWFs in Figure 6 to compare the differential behaviors of shot noise by employing equation (16). Figure 6a represents the conductance under the irradiation of MWFs with the commensurate numbers $q = 1$ and $q = 2$ as $\lambda_1 = 0.8$. We see that the multi-peaks are located at the absorbed and emitted photon numbers n, and the resonant structure exhibits asymmetric configuration about eV for the case of $q = 2$. The heights of peaks do not decline as eV increases as usual for the system perturbed by single MWF, but the peak at $n = 1$ is smaller than the peak at $n = 2$ for the solid curve. This suppression of peak results from the common effects of the applied two commensurate fields. However, for the case with commensurate number $q = 1$, the differential conductance appears symmetric behavior, and the multiple resonant behavior is exhibited evidently by the dotted curve. The two commensurate fields with the same frequency causes more elegant resonant structure, and the central peak is suppressed. This means that in the absence of MWFs, there exists a resonant peak located at $eV = 0$, but the conductance peak becomes a valley of two peaks with the energy gap about 2Δ. We refer it as the channel blockade due to multi-photon irradiation. This effect can be realized by analyzing the conductance formula given by equation (16). For the double fields applied system, many photon absorption and emission may contribute to the channel $E_d + p\Delta$ under the requirement $w_{\{\tilde{m}\}} = (m_1 + m_2 q)\Delta = p\Delta$ in equation (16), where p in an integer representing the rearranged resonant channels due to the applied ac fields within the regime $-\infty < p < \infty$. This condition gives the relation $m_2 = p - m_1$ for the commensurate fields applied system as $q = 1$. Substituting this relation into equation (16) we have conductance magnitude of the pth side photon level $\widetilde{G} = \frac{dI}{dV}|_p$ as

$$\widetilde{G} = G(p)\Big[\sum_{m_1} J_{m_1}(\lambda_1) J_{p-m_1}(\lambda_2)\Big]^2, \qquad (17)$$

where $G(p) = G_0 T_{LR}(eV - p\Delta)$. Employing the sum rule for the Bessel functions of the first kind, we obtain the exact expression related to the Bessel function by $\widetilde{G} = G(p) J_p^2(\Lambda)$, where $\Lambda = \lambda_1 + \lambda_2$. We therefore find that if Λ is a zero of the Bessel function $J_p(\Lambda)$, i.e., $J_p(\Lambda) = 0$, we have the zero conductance at the pth side photon level $p\Delta$ whenever the original conductance is. This means that if the system possesses a channel at E_d, the multi-photon absorption procedure makes this channel to be blockaded. In fact, $\Lambda \approx 2.4048$ and $\Lambda \approx 5.5201$ are the two zeros of $J_0(\Lambda)$. Actually, the parameters of the dotted curve in diagram (a) is $\lambda_1 = 0.8$, $\lambda_2 = 1.6$, and hence $\lambda_1 + \lambda_2 = 2.4$ is a zero of the Bessel function $J_0(\Lambda)$. Therefore, the original channel $E_d = 0$ is blockaded to form zero conductance at $eV = 0$. As the magnitudes of the fields increase to $\lambda_1 = 1.8$ and $\lambda_2 = 3.6$, the magnitude $\Lambda = 5.4$ approaches to another zero of the Bessel function $J_0(\Lambda)$, we therefore obtain the conductance shown by the dotted curve in diagram (b) for $q = 1$. For this case the zero channel of the field is also blockaded. The side peaks are larger than the central peaks, however the symmetric structure remains. As the magnitudes of the fields λ_1 and λ_2 are large ($\lambda_1 = \lambda_2 = 1.8$), one observes that the differential conductance for the case as $q = 2$ is modified considerably compared with the solid curve in diagram (a). The central peak is suppressed to a small value,and many novel side peaks appear asymmetric structure. Compared with the differential shot noise of the systems for the cases of commensurate unbalanced case shown in Figure 4, and the commensurate balanced case shown in Figure 5, one recognizes that the differential shot noise and differential conductance behaves quite differently.

The magnitude of each resonant conductance peak is contributed by absorbing and emitting many photons of the two fields, and the compound effect makes the suppression and enhancement of the resonant peaks. The photon-blockade effect is evidently seen to exhibit symmetric structure, and the conductance is weighted by $J_p^2(\Lambda)$ shown in Figure 7. One observes that the conductance can be completely suppressed by the two fields for the case $q = 1$, and magnitude of the conductance may have several zeros as long as Λ is large enough. Therefore, we can adjust the amplitudes of the applied two fields as the switches to make a channel open or close through photon-blockade effect.

The Fano factor $F = S/2eI$ is defined to classify the Poissonian $F = 1$, sub-Poissonian $F < 1$, and super-Poissonian $F > 1$ shot noise compared with the Schottky formula. In Figure 8 we present the Fano factor F with

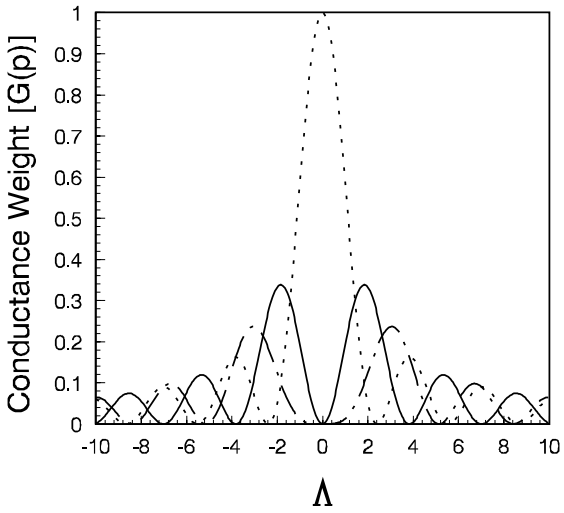

Fig. 7. The conductance weight $J_p^2(\Lambda)$ of system for $q = 1$. The parameter $\Lambda = \lambda_1 + \lambda_2$ controls the heights of the resonant peaks. The zeros of the curves are associated with the photon-blockade of the system. The dotted, solid, and dash-dotted curves are related to the magnitudes of the peaks located at $p = 0, \pm 1, \pm 2$, respectively.

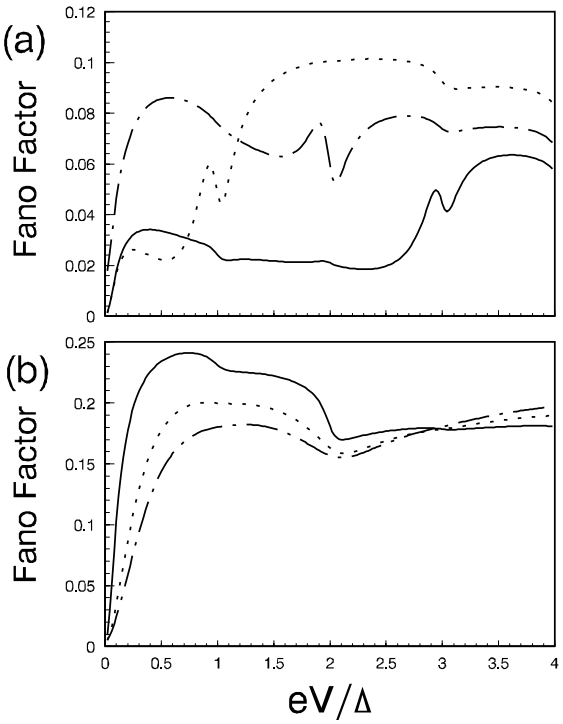

Fig. 8. The Fano factor versus source-drain bias eV for the commensurate balanced case. The parameters in diagram (a) are chosen as $\Gamma = 0.2\Delta$, $\lambda_1 = 1.5$, $\lambda_2 = 2\lambda_1/q$, and for the solid curve $q = 1$; for the dash-dotted curve $q = 2$; for the dotted curve $q = 3$. The parameters in diagram (b) are chosen as $q = 2$, $\lambda_1 = \lambda_2 = 0.8$, and for the solid, dotted, and dash-dotted curves $\Gamma = 0.2\Delta, 0.5\Delta, 0.7\Delta$, respectively.

respect to the source-drain bias eV for the commensurate balanced cases. The Fano factor increases from zero by increasing the source-drain bias to reach one of its extreme value, and then it declines to a valley. Several extreme values may exist in the larger region of source-drain bias. The detailed structure of Fano factor is sensitive to the commensurate number q of the system. We show the concrete behavior of the Fano factor in Figure 8a for different commensurate number $q = 1, 2, 3$. As $q = 1$, the Fano factor varies mildly in the region $0.4\Delta < eV < 2.6\Delta$, but it increases abruptly as $2.6\Delta < eV < 3.5\Delta$. However, for the case as $q = 3$, the Fano factor varies rapidly in the region $0.4\Delta < eV < 1.5\Delta$. The maximum value of the Fano factor also increases as q increases, say $F \approx 0.06$ for $q = 1$; $F \approx 0.084$ for $q = 2$; $F \approx 0.1$ for $q = 3$. We show the Fano factor with respect to the source-drain bias eV for choosing different values of line-width Γ in Figure 8b. One observes that the Fano factor is larger as the line-width Γ is larger in the region of source-drain bias $0 < eV < 3.0\Delta$, but it is smaller as the line-width is smaller in the region $eV > 3.0\Delta$. Since the Fano factor for the commensurate balanced absorption and emission system is smaller than one, the shot noise of this case belongs to the sub-Poissonian type of shot noise. The sensitive behaviors of Fano factor associated with different commensurate number, line-width, and the amplitudes of ac fields signify that the shot noise and tunneling current behave quite differently.

The Fano factor versus gate voltage V_g for the commensurate balanced and unbalanced absorption and emission procedures is displayed in Figure 9a and 9b, respectively. The dotted, solid curves in Figure 9a are depicted to associate with the commensurate number $q = 1, 2$, respectively. The Fano factor is smaller than one, and it exhibits rich concrete resonant structure related to eV_g for the balanced case. Different system under specific commensurate number q displays different configuration. The asymmetric behavior is strongly related to the commensurate number q, which indicates that we can suppress the shot noise by adjusting the commensurate number q and the gate voltage V_g even as the source-drain bias is large. The Fano factor for the commensurate unbalanced case can surpass one displayed in Figure 9b, i.e., the shot noise of this system can be located in the regime of super-Poissonian. The height of resonant peak is $F \approx 14.2$ for the system as $q = 1$, $eV = \Delta$. For the system as $q = 2$, and $eV = \Delta$, we have the height of resonant peak $F \approx 5.6$. In fact, the Fano factor for the commensurate unbalanced absorption and emission case is very large as the source-drain bias approaches zero. The cause of this situation is that as the source-drain bias $eV \to 0$, the shot noise reaches a definite value due to the correlations of photon-assisted tunneling currents shown in Figure 2. However, the time-averaged tunneling current approaches zero as $eV \to 0$ for our coupling system. The Fano factor is calculated from the shot noise divided by the tunneling current. Thus, if the current is small enough we can obtain the circumstance as $F \gg 1$.

4 Concluding remark

We have investigated the shot noise affected by the perturbation of two MWFs, which can be classified as the commensurate and incommensurate external ac fields. The

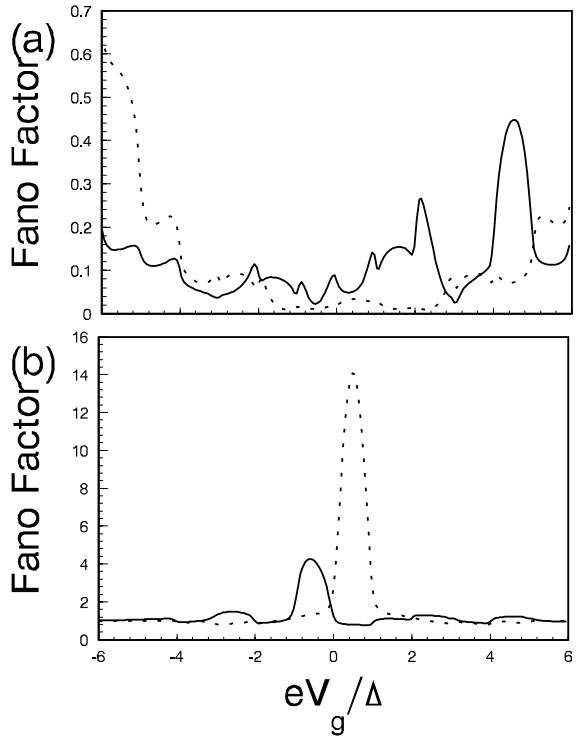

Fig. 9. The Fano factor versus gate voltage V_g for the commensurate balanced and unbalanced cases. The parameters are chosen as $eV = 1.0\Delta$, and $\Gamma = 0.2\Delta$. In diagram (a), $\lambda_1 = 1.5$, $\lambda_2 = 2\lambda_1/q$, and the dotted, solid curves are related to $q = 1, 2$, respectively. In diagram (b) $\lambda_1 = 0.8$, $\lambda_2 = 2\lambda_1/q$, and the dotted, solid curves are related to $q = 1, 2$, respectively.

current operator in the presence of external MWFs is derived using the equation of motion method, from which the device characteristics can be calculated, and the properties of applied fields, terminal features are involved in it. The current correlation function has been derived by evaluating their expectation and quantum average values. These current formula and current correlation functions are very different from the ones of single field applied system, which are nontrivial both for the tunneling current and the current noise. The current and the current-current correlations appear versatile oscillation due to the current branch interference and the applied ac fields. The shot noise spectral density is derived generally to fit the arbitrary applied double MWFs irradiating on the QD. The selection rule is found by considering the energy conservation associated with photon absorption and emission procedures during electrons transport through the system. This means that the MWFs irradiate the QD by transferring photon energy to the electrons in the QD, and the summation of absorbed photon energies from the two fields by the two correlated currents is equal to the emitted photon energies from the two correlated currents to the two MWFs. In order to obtain stable current correlations, several procedures may exist in the double MWFs irradiated system depending on the commensurate and incommensurate fields. The detailed approaches of absorption and emission of photons induce different kinds of noise spectral density. We have focused on the circumstance that the system is perturbed by the commensurate MWFs. Due to the perturbation of MWFs, the electron energy of the QD splits to form side-bands, and each corresponding side-channel is weighted by a Bessel function. The double commensurate MWFs may induce channel overlapping between different side-bands, and the weight functions produce unbalanced behaviors. From the selection rule, we find that the commensurate number q is involved in the numbers of absorbed and emitted photons by the restriction $m_1 + m_1' + (m_2 + m_2')q = n_1 + n_1' + (n_2 + n_2')q$. For this situation, $m_1 + m_1'$ and $n_1 + n_1'$ are the absorbed and emitted photon numbers in one field respectively, while $(m_2 + m_2')q$ and $(n_2 + n_2')q$ are the effective absorbed and emitted photon numbers in the other field respectively by taking one frequency ω_1 as the common frequency factor. This restriction also induces further asymmetrical behavior due to involving the tunneling weight functions associated with the Bessel functions in which the commensurate number q takes important role. The enhancement and suppression of photon-assisted noise spectral density therefore explicitly exhibited.

We have performed the numerical calculation for the cases of commensurate balanced and unbalanced photon absorption and emission based on the noise formulas given by equations (14) and (15). Different from the single MWF applied system, the quantum coherent current induces rich quantum correlation, and current noise is strongly affected by the external fields to exhibit different quantum structures. It is a consequence of the multi-photon absorption and emission procedure among different waves of electrons. The multi-photon process can be obviously seen from the resonance of shot noise, or from the differential conductance. Different commensurate number q contributes to different photon absorption and emission behaviors. The behaviors of commensurate balanced and unbalanced procedures result in quite different noise spectral density. For the balanced absorption procedure, the shot noise is zero in the absence of source-drain bias, and it increases as the absolute value of source-drain bias eV increases to exhibit stair-like behavior. For the double commensurate MWFs applied system, the shot noise is large enough to surpass its saturated value due to the unbalanced absorption and emission procedures. The shot noise contains rich structure as the source-drain bias is small, and the detailed photon-assisted behaviors disappear when the source-drain bias becomes large enough. The quantum behaviors induced by the photon absorption and emission become more evident as Γ becomes smaller. The sensitive behaviors of Fano factor associated with different commensurate number, line-width, and the amplitudes of ac fields signify that the shot noise and tunneling current behave quite differently. The shot noise related to the case of commensurate balanced absorption and emission belongs to the sub-Poissonian. The asymmetric behavior is strongly related to the commensurate number q. The Fano factor for the commensurate unbalanced case can surpass one. In fact, if the current is small enough

the Fano factor can be much larger than one. This kind of shot noise belongs to super-Poissonian.

The magnitude of differential conductance shows the nonlinear behavior of the system clearly due to the application of two commensurate fields. For the case with commensurate number $q = 1$, the differential conductance appears symmetric behavior, and the channel blockade exhibits due to the multi-photon absorption procedure. The noise possessing a gap for the commensurate balanced case as $q = 1$ indicates that the channel blockade takes place. We can adjust the amplitudes of the applied two fields to switch the channels through photon-blockade effect. Physically, the photon blockade effect can be understood by the situation that the applied two fields with the same frequency induce voltages on the gates. The voltages on the gates take the role for controlling the photon resonant conductance. The switching on and off the photon resonant conductance can be controlled exactly by changing the magnitudes of the applied potentials on the gate, i.e., as $\Lambda = \lambda_1 + \lambda_2$ is equal to one of the zeros of the Bessel function $J_p(\Lambda)$, the photon resonant conductance peak at $p\Delta$ is blockaded completely, and there is no electron tunneling in this channel. This effect allows us to contrive a photon-assisted electronic device to control the photon-electron tunneling channel exactly by adjusting the applied potential of ac fields. However for the case where $q > 1$, the peak suppression and enhancement induce asymmetric nonlinear differential conductance. We have compared the results with corresponding quantities in the system perturbed by single MWF, and realized that the system with double frequencies possesses richer physical behaviors than the one with single frequency. Our investigation involves the nonlinear and nonadiabatic photon-assisted transport, through which one recognizes that the multi-photon effects are important and many novel physically interested phenomena are contained in the compound system as the fields are strong.

This work was supported by a RGC grant from the SAR Government of Hong Kong under Grant No. HKU 7044/05P, LuXin Energy Group, by the National Natural Science Foundation of China under the Grant No. 10375007, and by the Fundamental Research Foundation of Beijing Institute of Technology under the Grant No. 1070050320705.

References

1. L.P. Kouwenhoven et al., Phys. Rev. Lett. **73**, 3443 (1994)
2. R.H. Blick et al., Appl. Phys. Lett. **67**, 3924 (1995)
3. C.A. Stafford, N.S. Wingreen, Phys. Rev. Lett. **76**, 1916 (1996)
4. C. Bruder, H. Schoeller, Phys. Rev. Lett. **72**, 1076 (1994)
5. H.K. Zhao, Z. Phys. B **102**, 415 (1997)
6. H.K. Zhao, Phys. Lett. A **226**, 105 (1997)
7. Q.F. Sun, T.H. Lin, Phys. Rev. B **56**, 3591 (1997)
8. M.H. Pedersen, M. Büttiker, Phys. Rev. B **58**, 12993 (1998)
9. V.S. Rychkov, M.L. Polianski, M. Büttiker, Phys. Rev. B **72**, 155326 (2005)
10. T. Kwapiński, R. Taranko, E. Taranko, Phys. Rev. B **72**, 125312 (2005)
11. M. Wagner, Phys. Rev. Lett. **76**, 4010 (1996)
12. R. Aguado, G. Platero, Phys. Rev. B **55**, 12860 (1997)
13. P.K. Tien, J.P. Gordon, Phys. Rev. **129**, 647 (1963)
14. L.P. Kouwenhoven et al., Surf. Sci. **361**, 591 (1996)
15. P.W. Brouwer, Phys. Rev. B **58**, R10135 (1998)
16. L.J. Geerligs et al., Phys. Rev. Lett. **64**, 2691 (1990)
17. M. Moskalets, M. Büttiker, Phys. Rev. B **69**, 205316 (2004)
18. M.M. Mahmoodian, L.S. Braginsky, M.V. Entin, Phys. Rev. B **74**, 125317 (2006)
19. M.M. Mahmoodian, M.V. Entin, EPL **77**, 67002 (2007)
20. Y.V. Nazarov, Physica B **189**, 57 (1993)
21. J. Lehmann, S. Kohler, P. Hänggi, J. Chem. Phys. **118**, 3283 (2003); F.J. Kaiser, S. Kohler, e-print `arXiv:cond-mat/0705.4204v1`; S. Kohler, J. Lehmann, P. Hänggi, Phys. Rep. **406**, 379 (2005)
22. A.P. Jauho, N.S. Wingreen, Y. Meir, Phys. Rev. B **50**, 5528 (1994)
23. H.K. Zhao, J. Wang, Phys. Rev. B **64**, 094505 (2001)
24. D.M. Basko, M.A. Skvortsov, V.E. Kravtsov, Phys. Rev. Lett. **90**, 096801 (2003)
25. M. Büttiker, Phys. Rev. Lett. **68**, 843 (1992); Phys. Rev. B **46**, 12485 (1992); Ya.M. Blanter, M. Büttiker, Phys. Rep. **336**, 1 (2000)
26. M.J.M. de Jong, C.W.J. Beenakker, Phys. Rev. B **46**, 13400 (1992); Phys. Rev. **49**, 16070 (1994)
27. B. Yurke, G.P. Kochanski, Phys. Rev. B **41**, 8184 (1990)
28. C.W.J. Beenakker, H. van Houten, Phys. Rev. B **43**, 12066 (1991)
29. J.H. Davies, P. Hyldgaard, S. Hershfield, J.W. Wilkins, Phys. Rev. B **46**, 9620 (1992)
30. U. Hanke, Y.M. Galperin, K.A. Chao, N. Zou, Phys. Rev. B **48**, 17209 (1993)
31. Q.F. Sun, J. Wang, T.H. Lin, Phys. Rev. B **61**, 13032 (2000)
32. R. Aguado, L.P. Kouwenhoven, Phys. Rev. Lett. **84**, 1986 (2000)
33. H.K. Zhao, Phys. Rev. B **63**, 205327 (2001); H.K. Zhao, J. Wang, Phys. Rev. B **74**, 245401 (2006)
34. G.B. Lesovik, L.S. Levitov, Phys. Rev. Lett. **72**, 538 (1994)
35. Y.P. Li, A. Zaslavsky, D.C. Tsui, M. Santos, M. Shayegan, Phys. Rev. B **41**, 8388 (1990)
36. M. Henny, S. Oberholzer, C. Strunk, C. Schönenberger, Phys. Rev. B **59**, 2871 (1999)
37. A.N. Korotkov, K.K. Likharev, Phys. Rev. B **61**, 15975 (2000)
38. G. Iannaccone, G. Lombardi, M. Macucci, B. Pellegrini, Phys. Rev. Lett. **80**, 1054(1998)
39. V.V. Kuznetsov, E.E. Mendez, J.D. Bruno, J.T. Pham, Phys. Rev. B **58**, R10159 (1998)
40. Ya.M. Blanter, M. Büttiker, Phys. Rev. B **59**, 10217 (1999)
41. H.K. Zhao, Commun. Theor. Phys. (Beijing) **33**, 341 (2000)
42. P.S.S. Guimarães et al., Phys. Rev. Lett. **70**,3792 (1993)
43. A.P. Jauho, N.S Wingreen, Phys. Rev. B **58**, 9619 (1998)
44. Z. Ma, Y. Zhu, X.Q. Li, T.H. Lin, Z.B. Su, Phys. Rev. B **69**, 045302 (2004)
45. R. Landauer, IBM J. Res. Dev. **1**, 223 (1957); M. Büttiker, Phys. Rev. Lett. **57**, 1761 (1986)
46. F. Simmel, R.H. Blick, J.P. Kotthaus, W. Wegscheider, M. Bichler, Phys. Rev. Lett. **83**, 804 (1999)